On the approximation of stable and unstable fiber bundles of (non)autonomous ODEs – a contour algorithm

Thorsten Hüls*
Department of Mathematics, Bielefeld University
POB 100131, 33501 Bielefeld, Germany
huels@math.uni-bielefeld.de

We propose an algorithm for the approximation of stable and unstable fibers that applies to autonomous as well as to nonautonomous ODEs. The algorithm is based on computing the zero-contour of a specific operator; an idea that was introduced in [Hüls, 2014] for discrete time systems. We present precise error estimates for the resulting contour algorithm and demonstrate its efficiency by computing stable and unstable fibers for a (non)autonomous pendulum equation in two space dimensions. Our second example is the famous three-dimensional Lorenz system for which several approximations of the two-dimensional Lorenz manifold are calculated. In both examples, we observe an equally well performance for autonomously and nonautonomously chosen parameters.

Keywords: Invariant fiber bundles, stable and unstable manifolds, numerical approximation, contour algorithm, Lorenz system.

AMS Subject Classification: 37C10, 34C45, 37B55.

1. Introduction

Stable and unstable manifolds provide a deep insight into the global dynamics of an autonomous ODE

$$x' = f(x), \quad f \in \mathcal{C}^1(\mathbb{R}^d, \mathbb{R}^d). \tag{1}$$

Denote by $\Upsilon(\cdot)$ its solution operator and let ξ be an equilibrium of (1). Stable and unstable manifolds are defined as

$$\begin{aligned} W^s(\xi) &= \{x \in \mathbb{R}^d : \lim_{t\to\infty} \Upsilon(t)x = \xi\}, \\ W^u(\xi) &= \{x \in \mathbb{R}^d : \lim_{t\to-\infty} \Upsilon(t)x = \xi\}. \end{aligned} \tag{2}$$

Various methods have been proposed for finding approximations of (2). We briefly list some of these approaches.

Several algorithm are based on numerical continuation techniques. Starting points are chosen from a local approximation, i.e. the tangent space, from which a global approximation is computed, see [Friedman & Doedel, 1991], [Johnson *et al.*, 1997], [Krauskopf & Osinga, 2003] and [Henderson, 2005]. The latter reference presents an algorithm that is based on computing two dimensional manifolds via so called fat trajectories.

The ansatz in [Guckenheimer & Vladimirsky, 2004] uses the fact that the vector field is tangent to the graph of the manifold. This results in a first-order quasilinear PDE that the authors solve efficiently to continue the manifold in this way.

Alternative approaches are based on set oriented methods, e.g. [Dellnitz & Hohmann, 1997] or on deriving Taylor expansions of the graph of the manifold, cf. [Simó, 1989], [Beyn & Kleß, 1998], [Eirola & von Pfaler, 2004].

We refer to [Krauskopf *et al.*, 2005] for a survey article that illustrates the application of selected

*Supported by CRC 701 'Spectral Structures and Topological Methods in Mathematics'.

techniques for computing the two-dimensional stable manifold of the fixed point $\xi = 0$ in the famous Lorenz system. This stable manifold is often referred to as the Lorenz manifold. Figure 1 shows this manifold, calculated with a variant of the method from [Johnson *et al.*, 1997].

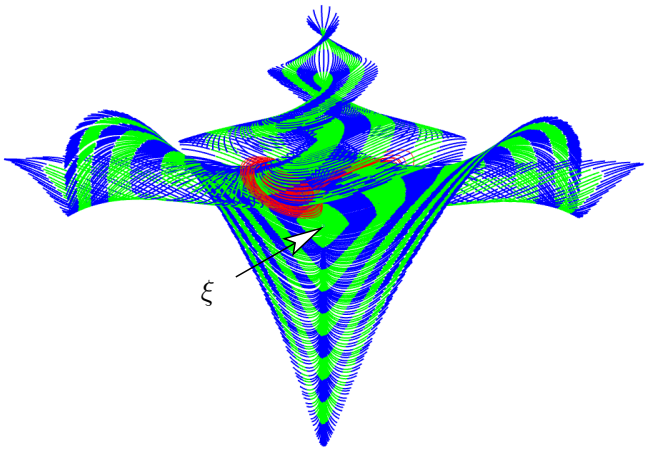

Fig. 1. Approximation of the Lorenz manifold and of the Lorenz attractor.

Real world systems almost always have time dependent influences, resulting in nonautonomous ODE models of the form

$$x' = F(t, x), \quad F \in \mathcal{C}^{0,1}(\mathbb{R} \times \mathbb{R}^d, \mathbb{R}^d). \qquad (3)$$

The development and analysis of a corresponding nonautonomous framework is currently an active field of research. Denote by $\Psi(\cdot,\cdot)$ the solution operator of (3), i.e $\Psi(s,t)x$ maps the initial point x at time t, to the solution at time s. In Section 2.1 we introduced assumptions that guarantee existence of these solutions. First note that a time independent equilibrium of (3) generally does not exist – its only meaningful replacement is a solution $\xi(\cdot)$ that is bounded on $\mathbb{R}$. Stable and unstable manifolds w.r.t. the solution $\xi(\cdot)$ are time variant sets that we call stable and unstable s-fibers, $s \in \mathbb{R}$, defined as

$$\mathcal{F}_s^+(\xi) = \{x \in \mathbb{R}^d : \lim_{t\to\infty} \|\Psi(t,s)x - \xi(t)\| = 0\},$$
$$\mathcal{F}_s^-(\xi) = \{x \in \mathbb{R}^d : \lim_{t\to-\infty} \|\Psi(t,s)x - \xi(t)\| = 0\}.$$

Alternatively, these sets are frequently denoted as *integral manifolds* in the literature.

The fact that unstable fibers are pullback attractors under reasonable assumptions, see [Aulbach *et al.*, 2006, Theorem 4.1], allows the application of set oriented methods for their computation. Reversing the direction of time, this approach yields an approximation of the stable fiber. Taylor expansions of fiber bundles are computed in [Pötzsche & Rasmussen, 2006] with special focus on obtaining coefficients of nonautonomous bifurcations. Finally, we refer to [Pötzsche & Rasmussen, 2009] and [Pötzsche & Rasmussen, 2010], where fiber approximations are derived via fixed points of the Lyapunov-Perron operator.

In this paper, we adapt a new ansatz to continuous time systems that was introduced in [Hüls, 2014] for the discrete time case. This approach is based on Hadamard's graph transform, cf. [Hadamard, 1901], [Katok & Hasselblatt, 1995, Theorem 6.2.8] and computes the zero-contour of a particular operator which results in an approximation of the desired fiber with high accuracy. The resulting contour algorithm uses available software for level sets. It is fast, easy to implement and error estimates justify its applicability. We demonstrate its power for a two-dimensional damped pendulum model as well as for the three-dimensional Lorenz system. For both models, we choose an autonomous and a nonautonomous parameter setup.

2. Approximation scheme

In this section, our approximation scheme and corresponding error estimates are presented. We begin with the introduction of the assumptions on the nonautonomous system (3).

2.1. *Assumptions*

Let us start with a motivation of our main assumptions **(A1)-(A3)** below. Although it is not a generic property, we assume without loss of generality that $\xi(t) = 0$ for all t, since F and the shifted equation

$$x' = G(t, x), \quad G(t, x) := F(t, x + \xi(t)) - F(t, \xi(t))$$

show the same dynamics. Furthermore, we assume that the equilibrium $\xi = 0$ is hyperbolic which formally can be expressed in terms of an exponential dichotomy of the variational equation

$$u' = D_x F(t, 0)u, \quad t \in \mathbb{R}. \qquad (4)$$

For readers, unfamiliar with this hyperbolicity concept, we refer to [Coppel, 1978, Section 2] and [Henry, 1981, Section 7.6].

Denote by d_s and d_u, $d_s + d_u = d$ the dimensions of the stable and the unstable subspace, respectively. In an autonomous setup, these subspaces are eigenspaces, while in nonautonomous systems, they are defined as the ranges of the stable and unstable dichotomy projectors. We assume without loss of generality that at each time instance, the stable subspace is aligned to the first d_s components

while the last d_u components belong to the unstable subspace. Note that a nonautonomous similarity transformation, cf. [Hüls, 2014, Sect. 4.2] – which does not change dynamics – always leads to this setup.

We apply the decomposition $x = \begin{pmatrix} x_s \\ x_u \end{pmatrix}$, $x_s \in \mathbb{R}^{d_s}$, $x_u \in \mathbb{R}^{d_u}$ and write our assumptions in terms of the solution operator of (3).

(A1) F satisfies assumptions, guaranteeing existence of solutions on the whole time interval. The solution operator Ψ satisfies the following uniform Lipschitz condition. On each compact set $\mathcal{K} \subset \mathbb{R}^d$ there exists a constant $L_{\mathcal{K}}$ such that

$$\|\Psi(t+h,t)x - \Psi(t+h,t)y\| \leq (L_{\mathcal{K}})^{|h|}\|x-y\|$$

for all $t, h \in \mathbb{R}$ and $x, y \in \mathcal{K}$.

(A2) $\Psi(t,s)x = \begin{pmatrix} A^s(t,s)x_s + f^s(t,s,(x_s,x_u)) \\ A^u(t,s)x_u + f^u(t,s,(x_s,x_u)) \end{pmatrix}$ for all $t, s \in \mathbb{R}$, $x \in \mathbb{R}^d$. Here $A^s(t,s) \in \mathbb{R}^{d_s,d_s}$, $A^u(t,s) \in \mathbb{R}^{d_u,d_u}$ for all $t, s \in \mathbb{R}$. For any $t, s \in \mathbb{R}$ the maps $f^{s,u}(t,s,\cdot) \in \mathcal{C}^1(\mathbb{R}^d, \mathbb{R}^{d_{s,u}})$ satisfy $f^{s,u}(t,s,0) = 0$ and $D_x f^{s,u}(t,s,0) = 0$. For arbitrary $\varepsilon > 0$ there exist $\gamma > 0$ and a neighborhood U of 0 such that $\|D_x f^{s,u}(t,s,x)\| \leq \varepsilon$ for all $x \in U$, $|t-s| \leq \gamma$, $t, s \in \mathbb{R}$.

(A3) Denote by Φ the solution operator of the variational equation (4) and define the projectors

$$P^s = \begin{pmatrix} I_{d_s} & 0 \\ 0 & 0 \end{pmatrix}, \quad P^u = \begin{pmatrix} 0 & 0 \\ 0 & I_{d_u} \end{pmatrix},$$

where $I_{d_{s,u}}$ denotes the identity in $\mathbb{R}^{d_{s,u}}$, respectively. There exist constants $K, \alpha_{s,u} > 0$ such that

$$\|\Phi^s(t,s)P^s\| \leq K\mathrm{e}^{-\alpha_s(t-s)},$$
$$\|\Phi^u(s,t)P^u\| \leq K\mathrm{e}^{-\alpha_u(t-s)}$$

for all $t \geq s$, $t, s \in \mathbb{R}$.

Remark 2.1. For arbitrary systems, approximate dichotomy projectors, specifying stable and unstable subspaces, can actually be computed efficiently. The algorithm, proposed in [Hüls, 2010, Section 2.3] applies to the h-flow of (3) and calculates these projectors by solving a linear least squares problem.

Algorithms that are based on SVD- and QR-decompositions are used in [Dieci *et al.*, 2010] to identify dichotomy spectra as well as stable and unstable subspaces.

Finally, we note that the strong assumption of an exponential dichotomy on $\mathbb{R}$ in **(A3)** is for convenience only. Indeed, it suffices to demand a half-sided dichotomy on some interval, unbounded above (below) for computing stable (unstable) fibers.

2.2. *Approximation Theorem*

At a fixed time $s \in \mathbb{R}$, we aim for an approximation of $\mathcal{F}_s^{\pm}(\xi)$ (below, we skip the argument (ξ)). First, we define the following sets with $r, t \in \mathbb{R}_+$:

$$\mathcal{U}^+_{s,r,t} = \{x \in \mathbb{R}^d : \Psi(s+\tau+r,s)x \in \mathcal{B}_\delta \forall 0 \leq \tau \leq t\},$$
$$\mathcal{V}^+_{s,r,t} = \{x \in \mathbb{R}^d : \big(\Psi(s+t+r,s)x\big)_u = 0\},$$
$$\mathcal{U}^-_{s,r,t} = \{x \in \mathbb{R}^d : \Psi(s-\tau-r,s)x \in \mathcal{B}_\delta \forall 0 \leq \tau \leq t\},$$
$$\mathcal{V}^-_{s,r,t} = \{x \in \mathbb{R}^d : \big(\Psi(s-t-r,s)x\big)_s = 0\}.$$

Here, $\mathcal{B}_\delta := \{x \in \mathbb{R}^d : \|x\| \leq \delta\}$ and "$)_{s,u}$" denotes the projection to the s and u component, respectively.

It turns out that

$$\mathcal{T}^+_{s,r,t} := \mathcal{U}^+_{s,r,t} \cap \mathcal{V}^+_{s,r,t} \quad \text{and} \quad \mathcal{T}^-_{s,r,t} := \mathcal{U}^-_{s,r,t} \cap \mathcal{V}^-_{s,r,t}$$

define good approximations of the stable and unstable s-fibers $\mathcal{F}^+_s$ and $\mathcal{F}^-_s$, respectively.

Indeed, we obtain upper-semicontinuity w.r.t. the Hausdorff semi-distance $\mathrm{dist}(A,B) := \sup_{a\in A}\inf_{b\in B}\|a-b\|$.

Theorem 1. *Assume **(A1)-(A3)**. For any $0 < \tilde{\alpha}_s < \alpha_s$, $0 < \tilde{\alpha}_u < \alpha_u$ there exist a $\delta > 0$ and constants $C > 0$, $\beta > 0$ such that for all $s \in \mathbb{R}$ and all $t, r \in \mathbb{R}_+$ we get*

$$\begin{aligned} \mathrm{dist}(\mathcal{T}^+_{s,r,t}, \mathcal{F}^+_s) &\leq C\mathrm{e}^{\beta r}\mathrm{e}^{-(\tilde{\alpha}_s+\tilde{\alpha}_u)t}, \\ \mathrm{dist}(\mathcal{T}^-_{s,r,t}, \mathcal{F}^-_s) &\leq C\mathrm{e}^{\beta r}\mathrm{e}^{-(\tilde{\alpha}_s+\tilde{\alpha}_u)t}. \end{aligned} \tag{5}$$

Proof. Without loss of generality assume that $t = \frac{t_1}{t_2}$, $r = \frac{r_1}{r_2}$ with $t_{1,2}, r_{1,2} \in \mathbb{N}$. Then the proof follows along the lines of [Hüls, 2014, Theorem 4] with the setting $k = 0$, $p = r_1 t_2$, $m = r_2 t_1$ and $F_n = \Psi(s+(n+1)h, s+nh)$ with $h = \frac{1}{r_2 t_2}$, $n = 0, \ldots, r+m$ in case of stable fibers. Note that it is an important consequence of **(A1)** that the s-fiber $\mathcal{F}^+_s$ and the corresponding k-fiber $\mathcal{F}^+_k$ of the h-flow coincide.

In the unstable case, we change the direction of time by iterating with $F_n = \Psi(s-(n+1)h, s-nh)$. Further note that the constant β is chosen as $\beta = |h| \log L_{\mathcal{K}}$, where $\mathcal{K}$ is a sufficiently large compact set, satisfying $T^{\pm}_{s,r,t} \subset \mathcal{K}$. ∎

2.3. *Numerical recipe*

We now turn the results from Theorem 1 into a numerical recipe.

The set $\mathcal{T}^+_{s,r,t}$, which yields an approximation of $\mathcal{F}^+_s$, has two additional parameters r and t. The parameter r controls the length of the computed fiber and the error estimate (5) shows that the parameter t controls the accuracy of this approximation.

Numerically, we approximate $\mathcal{V}^+_{s,r,t}$ by calculating the zero-contour of the operator

$$H^+(x) = \big(\Psi(s+t+r,s)x\big)_u$$

and in case of $\mathcal{V}^-_{s,r,t}$, we consider the operator

$$H^-(x) = \big(\Psi(s-t-r,s)x\big)_s.$$

Determining this contour is the main idea, giving the proposed method its name: *Contour algorithm.*

In stable and unstable cases, we restrict ourselves to $d-1$-dimensional fibers with $d \in \{2,3\}$. On a rectangle (cuboid) we define a sufficiently fine grid and compute – in a first step – for all grid points the corresponding values of $H^\pm$. In a second step, the MATLAB routine `contour` (space dimension $d=2$) and `isosurface` ($d=3$), respectively, applies to these data and determines the desired approximation of $\mathcal{V}^\pm_{s,r,t}$. Note that the computation of $H^\pm(x)$ for all points x on the grid can easily be parallelized, using vectorization techniques in MATLAB, resulting in a rather efficient algorithm.

So far, we only considered the set $\mathcal{V}^\pm_{s,r,t}$, which often yields a good approximation of $\mathcal{T}^\pm_{s,r,t}$. But if artifacts occur, see Section 3.1 for an example, one additionally has to verify, whether the computed points lie in $\mathcal{U}^\pm_{s,r,t}$.

We note that the final implementation of the contour algorithm directly applies to the original system. It is not necessary first to transform the bounded trajectory $\xi(\cdot)$ to the origin and to align the dichotomy subspaces as described in the beginning of Section 2.1. This transformation is introduced for clarity of presentation only. Alternatively, one can include these transformation steps directly in the definition of $\mathcal{T}^\pm_{s,r,t}$, see [Hüls, 2014, Section 4.1] for details in the discrete time case.

For solving ODEs numerically, we apply the classical Runge-Kutta scheme with step size h which is a forth order explicit one-step method. In case of stable fibers, we choose a positive step size $h>0$, while unstable fibers require negative step sizes $h<0$. With n, we denote the number of h-steps. Then $n\cdot|h|$ corresponds to $t+r$ in the definition of $H^\pm$. Thus, n and h are two relevant parameters for controlling the accuracy of our algorithm.

A third parameter that influences the quality of the output is the number of grid points, on which we evaluate $H^\pm$. For two-dimensional examples, we choose a grid of size 1500×1000 and in a three-dimensional space, the grid size is $400\times 400\times 400$.

3. Application

We apply our algorithm for computing stable and unstable fiber bundles to two examples. The first one is a pendulum equation with damping that we rewrite as a first order system of dimension two. The second example is the famous Lorenz system [Lorenz, 1963]. We particularly compute the Lorenz manifold in a small neighborhood of the attractor. For both examples, an autonomous as well as a nonautonomous setup of parameters is considered.

3.1. *Autonomous pendulum equation*

Consider the ODE

$$\begin{pmatrix}x_1\\x_2\end{pmatrix}' = \begin{pmatrix}x_2\\-\lambda x_2-\sin(x_1)\end{pmatrix}, \qquad \lambda = 0.1. \tag{6}$$

We start with the unstable manifold of the fixed point $\xi = \begin{pmatrix}\pi\\0\end{pmatrix}$ and apply the contour algorithm. Note that one-dimensional stable (unstable) manifolds can easily be calculated numerically via backward (forward) orbits with starting points on the stable (unstable) subspace. Nevertheless, we select this autonomous example for illustrating our algorithm before we turn to more challenging nonautonomous and three-dimensional cases.

We choose the step size $h=-0.1$ and iterate $n=300$ steps with the classical Runge-Kutta scheme to obtain an approximation of H^-. Figure 2 shows the graph of H^-.

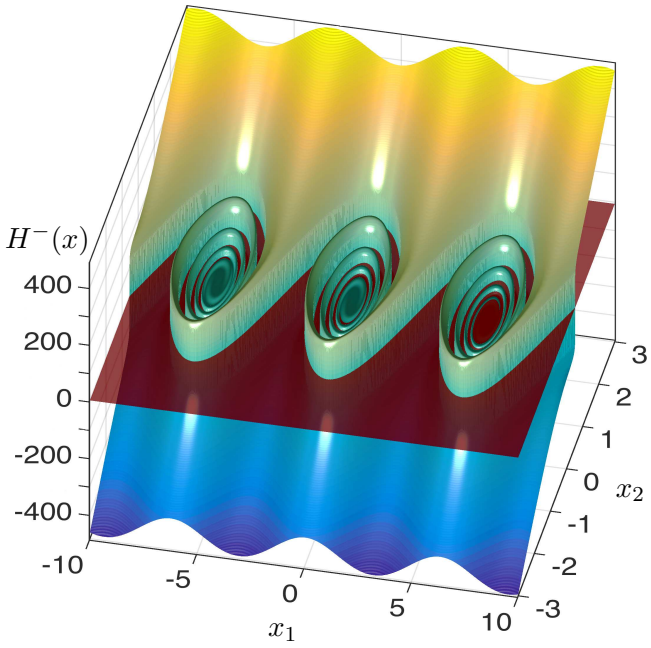

Fig. 2. Graph of H^- for $h = -0.1$ and $n = 300$.

The corresponding zero-contour of H^- is given in Fig. 3. One clearly observes the occurrence of numerical artifacts (gray points in Fig. 3). Indeed, these gray points lie on the unstable manifolds of adjacent saddles $\begin{pmatrix}(2k+1)\pi\\0\end{pmatrix}$, $k \neq 0$, $k \in \mathbb{Z}$.

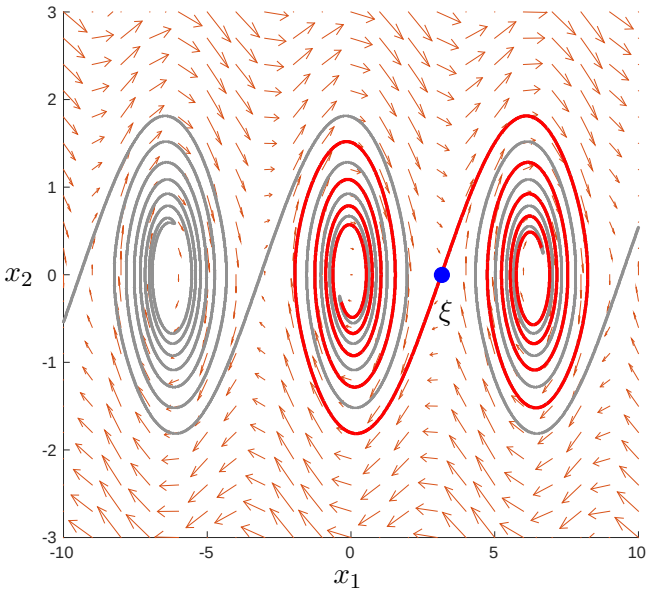

Fig. 3. Zero-contour of H^-. The gray points are numerical artifacts that do not lie in $\mathcal{U}^-_{s,r,t}$.

Note that the computed points lie in $\mathcal{V}^-_{s,r,t}$, but not necessarily in $\mathcal{U}^-_{s,r,t}$ and therefore not necessarily in $\mathcal{T}^-_{s,r,t}$. Respecting this second condition, we avoid artifacts by deleting any point from the contour whose backward orbit does not intersect a sufficiently small neighborhood of the fixed point ξ. In this way, the gray points are deleted from the approximate fiber in Fig. 3.

Figure 4 shows the stable manifold in green, computed with step size $h = 0.1$ and $n = 50$ iteration steps, while for the unstable manifold, we choose $h = -0.1$ and $n = 600$ iteration steps.

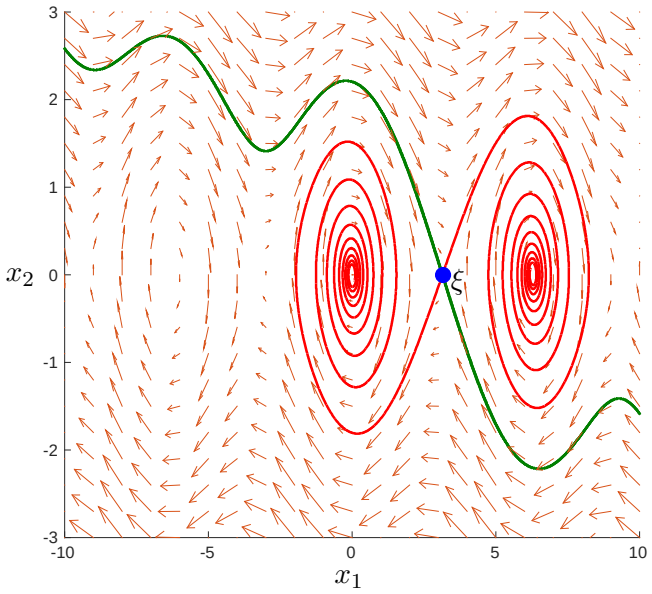

Fig. 4. Approximation of the stable (green) and unstable (red) manifold of the fixed point ξ.

3.2. *Nonautonomous pendulum equation*

We introduce a time dependent modification of (6):

$$\begin{pmatrix}x_1\\x_2\end{pmatrix}' = \begin{pmatrix}x_2\\-\left(0.6\sin(\frac{\pi}{100}t)+0.7\right)x_2 - \sin(x_1)\end{pmatrix}.$$

The periodic choice of the time dependent influence is for convenience only. Note that the period is rather long and that the contour algorithm makes no use of any periodicity.

This systems still has the time independent fixed point $\xi = 0$. In Fig. 5, we compute stable and unstable s-fibers for $s = 50 + 20k$ and $k \in \{0, 1, \ldots, 6\}$. For each stable fiber we choose $h = 0.1$ and $n = 100$, while in the unstable case $h = -0.1$ and $n = 300$.

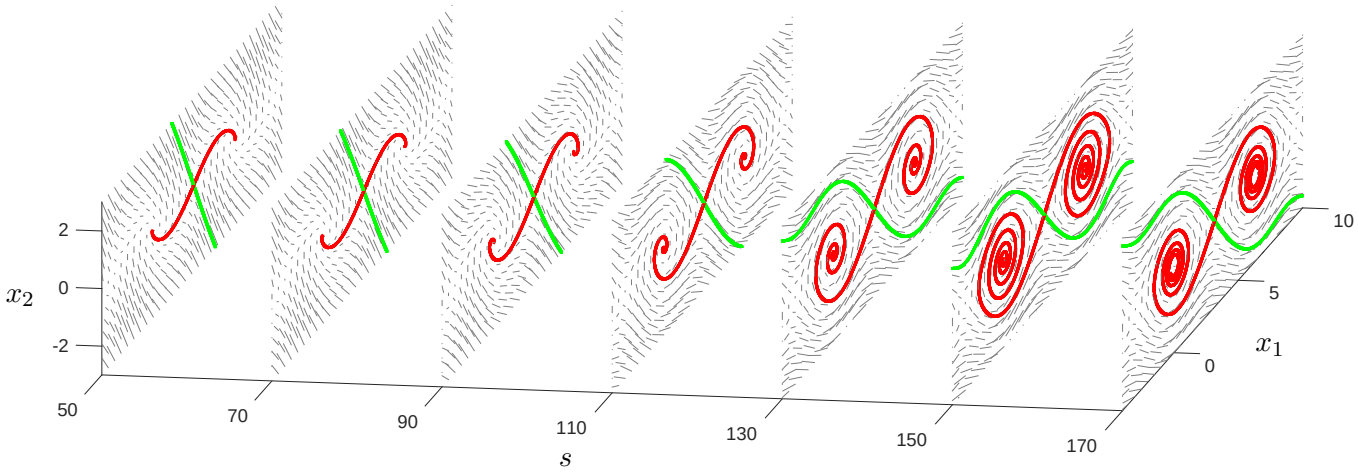

Fig. 5. Stable (green) and unstable (red) s-fibers of the fixed point ξ.

The nonautonomous parameter $0.6\sin(\frac{\pi}{100}s) + 0.7$ is minimal for $s = 150 + 200\ell$ and maximal for $t = 50 + 200\ell$, $\ell \in \mathbb{Z}$. Consequently, the shape of the s-fibers significantly differs at these extreme values.

In Fig. 6 we plot stable and unstable s-fibers for $s \in \{140, 145, 150\}$. Two trajectories illustrate that these fibers are invariant in the sense that $x \in \mathcal{F}_s^{\pm}$ if and only if $\Psi(t+s, s)x \in \mathcal{F}_{s+t}^{\pm}$.

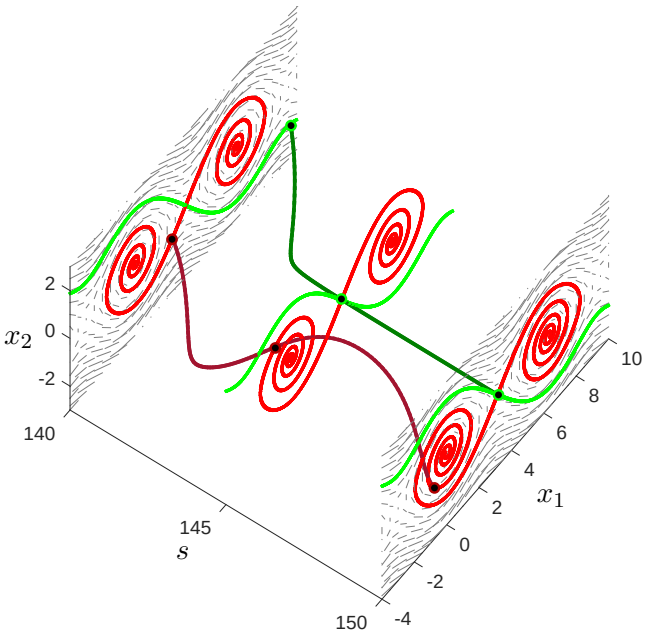

Fig. 6. Stable (green) and unstable (red) s-fibers of the fixed point ξ and two trajectories on these fibers.

Finally, we refer to an alternative ansatz for computing one-dimensional fibers in two-dimensional systems. The authors of [Mancho *et al.*, 2003] calculate stable (unstable) fibers at time t by starting with a local approximation at time $t + \tau$, $(t - \tau)$ for $\tau > 0$ sufficiently large. A continuation of this local segment backward (forward) in time leads to the desired approximation.

3.3. *The Lorenz manifold*

In this section, we consider the three-dimensional Lorenz system, cf. [Lorenz, 1963]

$$\begin{pmatrix} x_1 \\ x_2 \\ x_3 \end{pmatrix}' = \begin{pmatrix} \sigma(x_2 - x_1) \\ \varrho x_1 - x_2 - x_1 x_3 \\ x_1 x_2 - \beta x_3 \end{pmatrix}$$

with parameter setup

$$\sigma = 10, \quad \varrho = 28, \quad \beta = \tfrac{8}{3}.$$

We are interested in visualizing the Lorenz manifold, i.e. the two-dimensional manifold of the equilibrium $\xi = 0$. Figure 1 shows an approximation of this manifold and of the Lorenz attractor. This approximation of the Lorenz manifold was achieved by computing sufficiently many trajectories with starting points on a small circle, lying in the stable subspace, see [Johnson *et al.*, 1997].

The overview article [Krauskopf *et al.*, 2005] compares five different methods for the approximation of this manifold. These methods are base on

- computing geodesic level sets,
- continuation of trajectories via boundary value problems,
- computation of so called fat trajectories,
- solving first order quasilinear PDEs, resulting from the fact that the vector field is tangent to the graph of the manifold,

• finding a box covering of the Lorenz manifold, using set oriented algorithms.

We are particularly interested in the Lorenz manifold in a neighborhood of the attractor and aim for an illustration of its leafs, cutting through the attractor without intersecting it. For this task, we apply the contour algorithm with $h = 0.02$ and $n = 100$, see Fig. 7.

The colors in this figure are chosen from yellow to blue, depending on the value of x_1. A similar color coding with respect to one coordinate is used in all figures below.

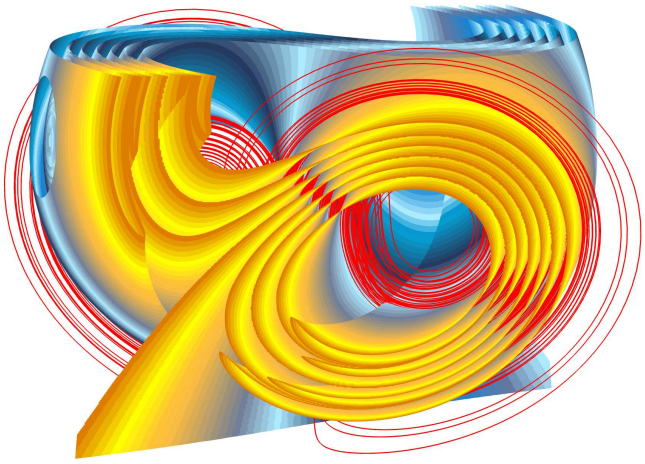

Fig. 7. Approximation of the Lorenz manifold in a neighborhood of the attractor.

For a study of the manifold close to the attractor in more detail, we cut away parts of this manifold that obstruct the view on the attractor. Numerically, we proceed the other way round by choosing three boxes on which we recompute the Lorenz manifold, applying the contour algorithm. Figure 8 shows these boxes together with the approximate manifolds.

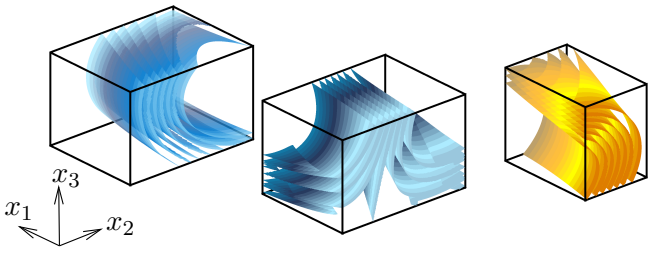

Fig. 8. The Lorenz manifold in three areas close to the attractor.

In combination with the Lorenz attractor, the local approximations from Fig. 8 are depicted in Fig. 9.

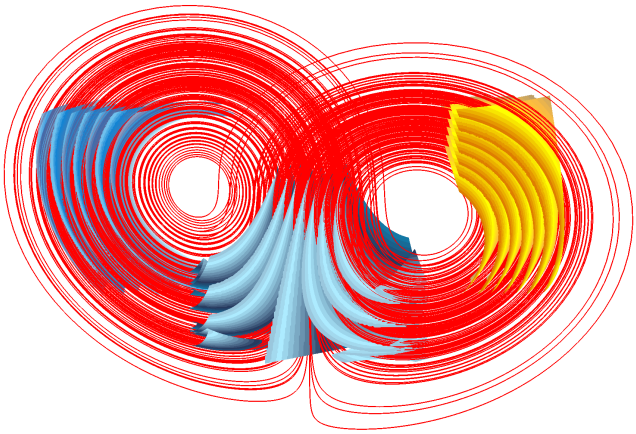

Fig. 9. The Lorenz manifold in three areas close to the attractor.

These figures illustrate a fundamental difference between the contour algorithm and continuation techniques. For the computation of Fig. 7, the contour method iterates each grid-point in the given box for 100 steps. Then the resulting information is used to approximate the graph of the stable manifold with high resolution. Furthermore, whether the fixed point lies in the starting box or at great distance from it, is irrelevant for this algorithm. Note that the manifold is not computed up to a fixed length in a dynamic of geodesic sense. This can be achieved, using continuation techniques that start in a small neighborhood of the fixed point and grow the manifold from these starting points. Consequently, the output of the contour algorithm differs from the continuation picture in Fig. 1.

For an illustration, we apply the contour algorithm on the box $[-70, 70] \times [-70, 70] \times [-125, 125]$ with $n = 50$. Figure 10 shows the resulting surface that we plot semitransparently. In addition, the approximation from Fig. 1 is displayed and a careful inspection indicates that this approximation lies close to the surface, computed by the contour algorithm.

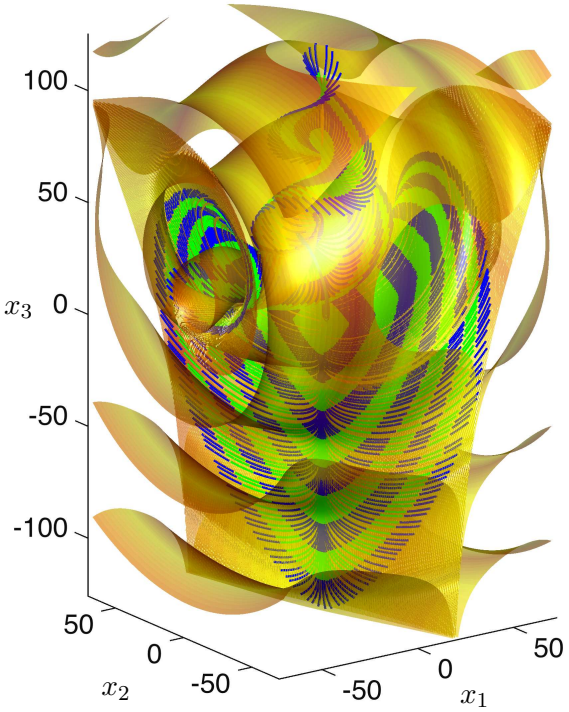

Fig. 10. Lorenz manifold, computed with the contour algorithm (semitransparent) and the alternative approximation from Fig. 1.

We demonstrate how the approximate manifolds depend on the number of iteration steps n. An application of the contour algorithm on the box $[-50, 50] \times [-50, 50] \times [-30, 27]$, yields an approximation similar to the one in [Henderson, 2005, Fig. 31]. In Fig. 11 and Fig. 12 we choose $n \in \{50, 75\}$, respectively.

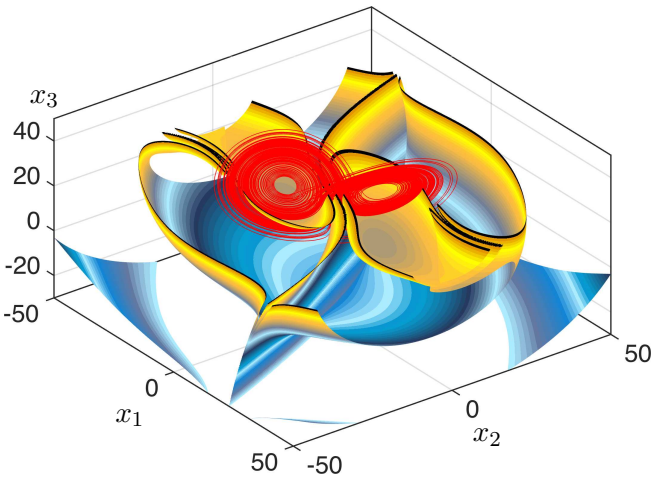

Fig. 11. Parts of the Lorenz manifold with $n = 50$.

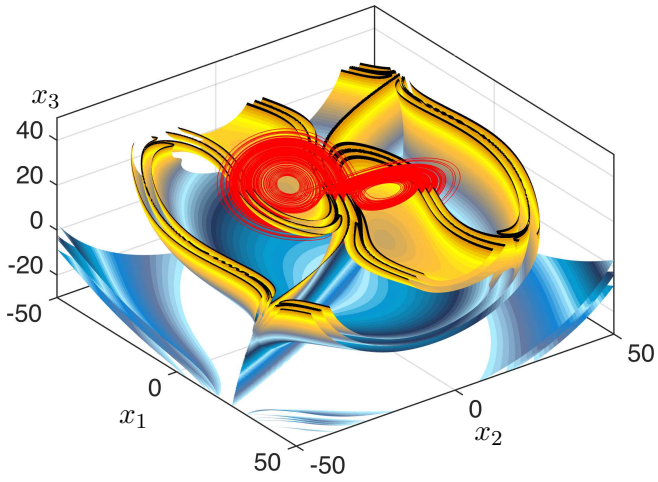

Fig. 12. Parts of the Lorenz manifold with $n = 75$.

Corresponding computations on the box $[-50, 50] \times [-50, 0] \times [-50, 100]$ with $n \in \{50, 100\}$, cf. [Henderson, 2005, Fig. 15(c)], are pictured in Fig. 13 and Fig. 14.

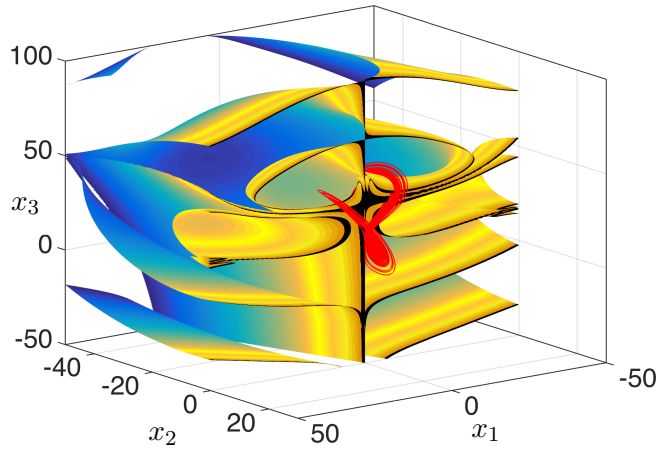

Fig. 13. Parts of the Lorenz manifold with $n = 50$.

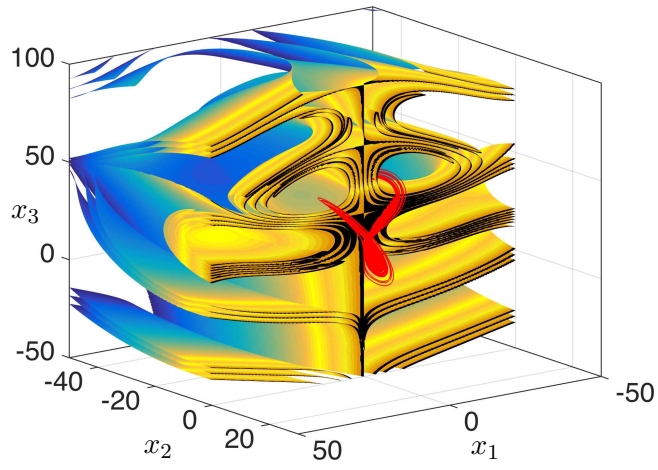

Fig. 14. Parts of the Lorenz manifold with $n = 100$.

3.4. *A nonautonomous Lorenz system*

We consider a nonautonomous generalization of the Lorenz system

$$\begin{pmatrix} x_1 \\ x_2 \\ x_3 \end{pmatrix}' = \begin{pmatrix} \sigma(x_2 - x_1) \\ \varrho x_1 - x_2 - x_1 x_3 \\ x_1 x_2 - \beta(t) x_3 \end{pmatrix} \tag{7}$$

with parameter setup

$$\sigma = 10, \quad \varrho = 28, \quad \beta(t) = \tfrac{8}{3}\left(1 - \sin(\tfrac{\pi}{10}t)\right),$$

cf. [Rasmussen, 2007, Example 7.14].

Figure 15 shows a local picture of the stable s-fibers for $s = 0$ and $s = 2$ in a neighborhood of the fixed point $\xi = 0$. For their computation, we apply the contour algorithm on the box $[-10, 10]^3$ with $n = 100$. The point, marked in red in Fig. 15 (left), is mapped by the solution operator $\Psi(2, 0)$ into a tiny neighborhood of the fixed point ξ (right).

An application of the contour algorithm on the box $[-0, 50] \times [-50, 50] \times [-50, 100]$ with $n = 50$ yields a global picture of s-fibers with $s \in \{0, 2\}$, see Fig. 16.

3.5. *Computing time*

In this section, we comment on computing times of the contour algorithm. Recall that a fiber approximation requires the following steps:

(i) Iterate all points on the grid for a given number of Runge-Kutta steps and obtain a value table of $H^{\pm}$.

(ii) Use these data and the MATLAB commands `contour` and `isosurface`, respectively, to obtain the zero-contour of $H^{\pm}$.

For the numerical experiments in this article, we use MATLAB® R2015B on an Intel® Xeon® Processor E5-2670 with 2.6 GHz as base frequency.

The computation of the one-dimensional stable manifold in Fig. 4 took 7.5 s for step (i) and 0.05 s to execute the `contour` command in step (ii). The unstable manifold in this figure is more time consuming, since we iterate every point on the 1500×1000 grid for 600 Runge-Kutta steps: 93 s for step (i) and 0.8 s for step (ii). The additional check to avoid artifacts took 4.3 s.

The two-dimensional Lorenz manifold from Fig. 12 is approximated with $400 \times 400 \times 400$ grid points and 75 iterations. Step (i) took 1348 s and 267 s were needed to apply the `isosurface` command.

Finally, we emphasize a particular strength of the contour algorithm: It easily calculates fiber bundles in a nonautonomous model. Furthermore, the computational effort for a single nonautonomous fiber matches computing times for a manifold in an autonomous system.

The left fiber in Fig. 16 needed on a $400 \times 400 \times 400$ grid 975 s for the 50 iterations of step (i) and the `isosurface` command in step (ii) took 41 s. Corresponding times for the right fiber in Fig. 16 are 989 s and 88 s.

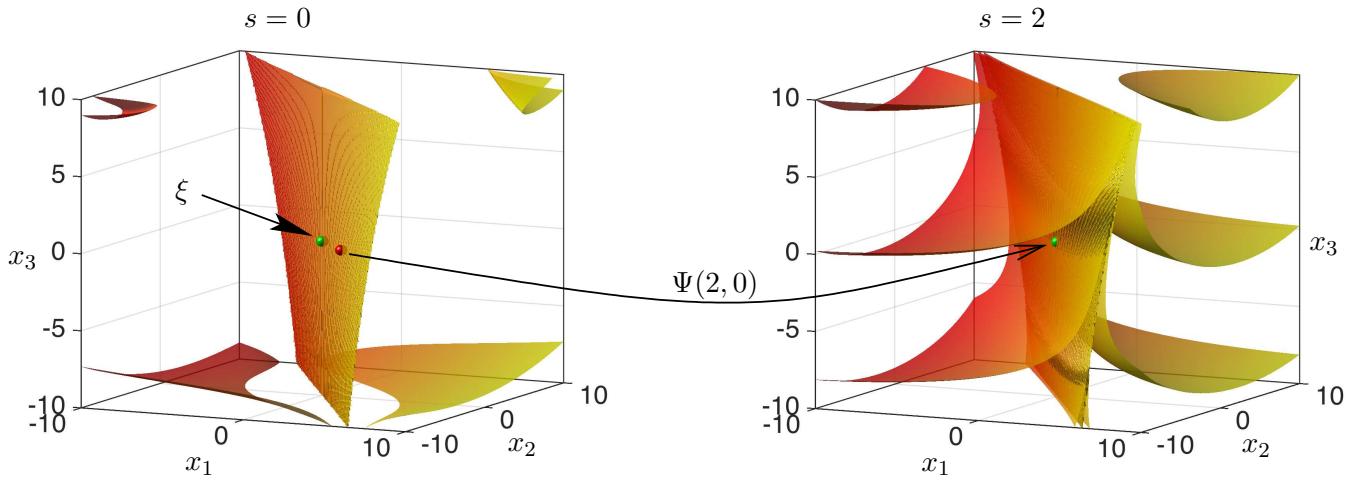

Fig. 15. Approximation of nonautonomous s-fibers of (7) for $s \in \{0, 2\}$.

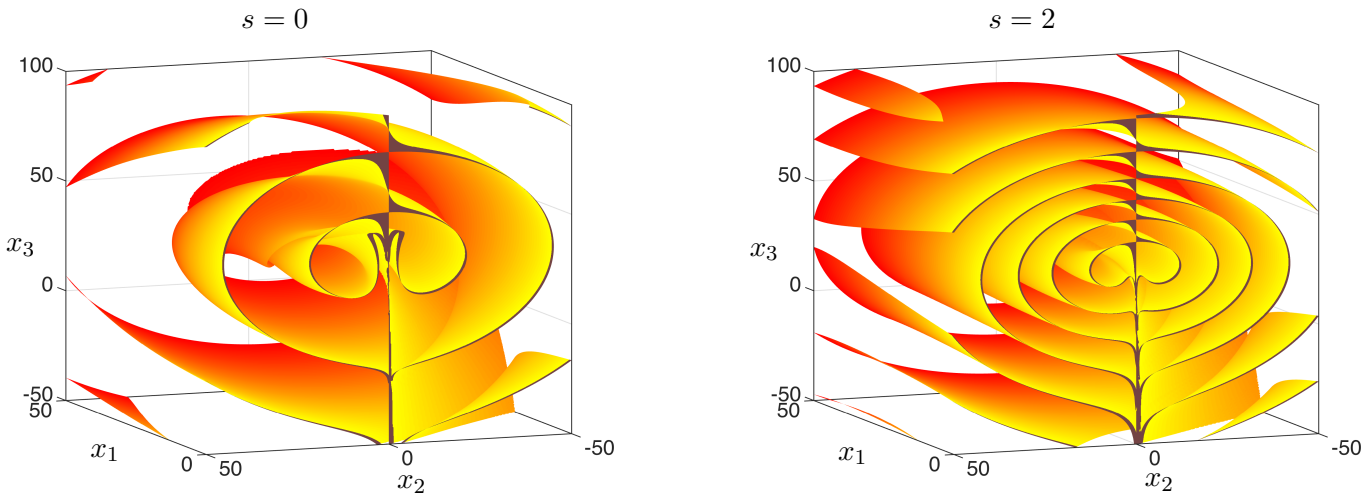

Fig. 16. Approximation of nonautonomous s-fibers of (7) for $s \in \{0, 2\}$.

References

Aulbach, B., Rasmussen, M. & Siegmund, S. [2006] "Invariant manifolds as pullback attractors of nonautonomous differential equations," *Discrete Contin. Dyn. Syst.* **15**, 579–596, doi:10.3934/dcds.2006.15.579.

Beyn, W.-J. & Kleß, W. [1998] "Numerical Taylor expansions of invariant manifolds in large dynamical systems," *Numer. Math.* **80**, 1–38, doi:10.1007/s002110050357.

Coppel, W. A. [1978] *Dichotomies in Stability Theory* (Springer-Verlag, Berlin), ISBN 3-540-08536-X, lecture Notes in Mathematics, Vol. 629.

Dellnitz, M. & Hohmann, A. [1997] "A subdivision algorithm for the computation of unstable manifolds and global attractors," *Numer. Math.* **75**, 293–317, doi:10.1007/s002110050240.

Dieci, L., Elia, C. & Van Vleck, E. [2010] "Exponential dichotomy on the real line: SVD and QR methods," *J. Differential Equations* **248**, 287–308, doi:10.1016/j.jde.2009.07.004.

Eirola, T. & von Pfaler, J. [2004] "Numerical Taylor expansions for invariant manifolds," *Numer. Math.* **99**, 25–46, doi:10.1007/s00211-004-0537-6.

Friedman, M. J. & Doedel, E. J. [1991] "Numerical computation and continuation of invariant manifolds connecting fixed points," *SIAM J. Numer. Anal.* **28**, 789–808.

Guckenheimer, J. & Vladimirsky, A. [2004] "A fast method for approximating invariant manifolds," *SIAM J. Appl. Dyn. Syst.* **3**, 232–260, doi:10.1137/030600179.

Hadamard, J. [1901] "Sur l'itératio et les solutions asymptotiques des équations différentielles," *Bull. Soc. Math. France* **29**, 224–228.

Henderson, M. E. [2005] "Computing invariant manifolds by integrating fat trajectories," *SIAM J. Appl. Dyn. Syst.* **4**, 832–882 (electronic), doi:10.1137/040602894.

Henry, D. [1981] *Geometric Theory of Semilinear Parabolic Equations* (Springer-Verlag, Berlin), ISBN 3-540-10557-3.

Hüls, T. [2010] "Computing Sacker-Sell spectra in discrete time dynamical systems," *SIAM J. Numer. Anal.* **48**, 2043–2064, doi:10.1137/090754509.

Hüls, T. [2014] "A contour algorithm for computing stable fiber bundles of nonautonomous, noninvertible maps," Tech. Rep. 14070, Bielefeld University, CRC 701.

Johnson, M. E., Jolly, M. S. & Kevrekidis, I. G. [1997] "Two-dimensional invariant manifolds and global bifurcations: some approximation and visualization studies," *Numer. Algorithms* **14**, 125–140, doi:10.1023/A:1019104828180.

Katok, A. & Hasselblatt, B. [1995] *Introduction to the modern theory of dynamical systems*, Encyclopedia of Mathematics and its Applications, Vol. 54 (Cambridge University Press, Cambridge), ISBN 0-521-34187-6, doi:10.1017/CBO9780511809187, with a supplementary chapter by Katok and Leonardo Mendoza.

Krauskopf, B. & Osinga, H. M. [2003] "Computing geodesic level sets on global (un)stable manifolds of vector fields," *SIAM J. Appl. Dyn. Syst.* **2**, 546–569 (electronic), doi:10.1137/030600180.

Krauskopf, B., Osinga, H. M., Doedel, E. J., Henderson, M. E., Guckenheimer, J., Vladimirsky, A., Dellnitz, M. & Junge, O. [2005] "A survey of methods for computing (un)stable manifolds of vector fields," *Internat. J. Bifur. Chaos Appl. Sci. Engrg.* **15**, 763–791, doi:10.1142/S0218127405012533.

Lorenz, E. N. [1963] "Deterministic nonperiodic flow," *J. Atmos. Sci.* **20**, 130–141.

Mancho, A. M., Small, D., Wiggins, S. & Ide, K. [2003] "Computation of stable and unstable manifolds of hyperbolic trajectories in two-dimensional, aperiodically time-dependent vector fields," *Phys. D* **182**, 188–222, doi:10.1016/S0167-2789(03)00152-0.

Pötzsche, C. & Rasmussen, M. [2006] "Taylor approximation of integral manifolds," *J. Dynam. Differential Equations* **18**, 427–460, doi:10.1007/s10884-006-9011-8.

Pötzsche, C. & Rasmussen, M. [2009] "Computation of nonautonomous invariant and inertial manifolds," *Numer. Math.* **112**, 449–483, doi:10.1007/s00211-009-0215-9.

Pötzsche, C. & Rasmussen, M. [2010] "Computation of integral manifolds for Carathéodory differential equations," *IMA J. Numer. Anal.* **30**, 401–430, doi:10.1093/imanum/drn059.

Rasmussen, M. [2007] *Attractivity and bifurcation for nonautonomous dynamical systems*, Lecture Notes in Mathematics, Vol. 1907 (Springer, Berlin).

Simó, C. [1989] "On the analytical and numerical approximation of invariant manifolds," *Les méthodes modernes de la mécanique céleste*, eds. Benest, D. & Froeschlé, C., pp. 285–329.